

PAPER

Probing negatively charged and neutral excitons in MoS₂/hBN and hBN/MoS₂/hBN van der Waals heterostructures

To cite this article: J Jadczyk *et al* 2021 *Nanotechnology* **32** 145717

View the [article online](#) for updates and enhancements.



IOP | ebooks™

Bringing together innovative digital publishing with leading authors from the global scientific community.

Start exploring the collection—download the first chapter of every title for free.

Probing negatively charged and neutral excitons in MoS₂/hBN and hBN/MoS₂/hBN van der Waals heterostructures

J Jadczyk^{1,*} , J Kutrowska-Girzycka¹ , M Bieniek^{2,3}, T Kazmierczuk⁴ , P Kossacki⁴ , J J Schindler⁵ , J Debus⁵ , K Watanabe⁶ , T Taniguchi⁶, C H Ho⁷ , A Wójs², P Hawrylak³ and L Bryja^{1,*} 

¹Department of Experimental Physics, Wrocław University of Science and Technology, Wybrzeże Wyspiańskiego 27, 50-370 Wrocław, Poland

²Department of Theoretical Physics, Wrocław University of Science and Technology, Wybrzeże Wyspiańskiego 27, 50-370 Wrocław, Poland

³Department of Physics, University of Ottawa, Ottawa, Ontario, K1N 6N5, Canada

⁴Institute of Experimental Physics, Faculty of Physics, University of Warsaw, Pasteura 5, 02-093 Warsaw, Poland

⁵Experimentelle Physik 2, Technische Universität Dortmund, 44227 Dortmund, Germany

⁶National Institute for Materials Science, Tsukuba, Ibaraki, 305-0044, Japan

⁷Department of Electronic Engineering, National Taiwan University of Science and Technology, Taipei, 106, Taiwan

E-mail: joanna.jadczyk@pwr.edu.pl and leszek.bryja@pwr.edu.pl

Received 14 July 2020

Accepted for publication 18 December 2020

Published 15 January 2021



CrossMark

Abstract

High-quality van der Waals heterostructures assembled from hBN-encapsulated monolayer transition metal dichalcogenides enable observations of subtle optical and spin-valley properties whose identification was beyond the reach of structures exfoliated directly on standard SiO₂/Si substrates. Here, we describe different van der Waals heterostructures based on uncapped single-layer MoS₂ stacked onto hBN layers of different thicknesses and hBN-encapsulated monolayers. Depending on the doping level, they reveal the fine structure of excitonic complexes, i.e. neutral and charged excitons. In the emission spectra of a particular MoS₂/hBN heterostructure without an hBN cap we resolve two trion peaks, T₁ and T₂, energetically split by about 10 meV, resembling the pair of singlet and triplet trion peaks (T_S and T_T) in tungsten-based materials. The existence of these trion features suggests that monolayer MoS₂ has a dark excitonic ground state, despite having a ‘bright’ single-particle arrangement of spin-polarized conduction bands. In addition, we show that the effective excitonic *g*-factor significantly depends on the electron concentration and reaches the lowest value of -2.47 for hBN-encapsulated structures, which reveals a nearly neutral doping regime. In the uncapped MoS₂ structures, the excitonic *g*-factor varies from -1.15 to -1.39 depending on the thickness of the bottom hBN layer and decreases as a function of rising temperature.

Keywords: transition metal dichalcogenides monolayers, molybdenum disulfide, exciton, trion, Zeeman *g*-factor

(Some figures may appear in colour only in the online journal)

* Authors to whom any correspondence should be addressed.

1. Introduction

Monolayer transition metal dichalcogenides (TMDs) have attracted considerable scientific interest due to their unique physical properties and foreseen applications in novel optoelectronics devices [1–3]. Unlike their bulk equivalents, indirect gap semiconductors, they possess direct optical bandgaps located at $\pm K$ valleys of the two-dimensional (2D) hexagonal Brillouin zone [4]. Additionally, the lack of inversion symmetry and strong spin–orbit coupling in the monolayer result in a substantial valley-contrasting spin-splitting of the valence and conduction bands [5]. The larger spin-splitting of the valence band (Δ_v) ranges from ~ 150 meV in MoS₂ to ~ 450 meV in WSe₂ and leads to the formation of so-called X_A and X_B excitons [6]. The conduction-band spin-splitting (Δ_c), predicted in numerical calculations [5], is appreciably smaller (up to few tens of meV) and exhibits a large relative difference, both in the energy and sign between different materials, and consequently imposes a splitting between the dark and bright exciton subbands. The bright excitons are composed of the electron from the conduction band and the hole from the valence band with the same spin, whereas dark excitons are composed of the electron and hole with the opposite spin. In monolayer WS₂ and WSe₂, Δ_c is predicted to be negative and the lowest energy exciton is dark. In monolayer MoSe₂, Δ_c is predicted to be positive and the lowest energy exciton is bright. Regarding monolayer MoS₂, the nature of the exciton is still controversial. Recent reports, including ours [7], have suggested that contrary to the ‘bright’ arrangement of the band structure, the strong exchange electron–hole interaction leads to the lowest energy for dark excitons [7–10].

The 2D character of monolayer TMDs and reduced dielectric screening allow for the formation of excitons with binding energies of a few hundreds of meV [8], orders of magnitude larger than those in typical quasi-2D quantum wells [11, 12]. In addition to neutral excitons, in the presence of excess carriers, trions can also be formed [13–18] with binding energies (E_B) of tens of meV, resulting in their stability even at room temperature [19–21]. Consequently, monolayer TMDs constitute a novel platform for optically probe many-body effects in the presence of strong Coulomb interactions [15, 22–26], particularly when the Fermi level in the conduction band for n-doped samples is lower or of the same order as the trion binding energy [27–29].

Monolayer MoS₂ is probably the best-known member of semiconducting TMDs [30] due to its natural abundance in almost chemically pure mineral molybdenite [31]. Compared to other materials from the MX₂ (M = Mo, W; X = S, Se, Te) family, MoS₂ is unique in having a small spin-splitting (~ 3 meV) of the conduction band [32], in comparison to typical Fermi energies in n-type exfoliated TMD monolayers (MLs) transferred onto standard SiO₂/Si substrates [3, 33]. Until recently, the optical quality of monolayer MoS₂ was inferior in quality to its related materials, such as MoSe₂, WS₂, and WSe₂. This allowed for observation of only broad photoluminescence peaks dominated by trions [19]. However, progress was made by the encapsulation of a MoS₂

monolayer with hexagonal boron nitride (hBN) layers, resulting in narrow neutral exciton lines with a width of about 2 meV at low temperatures (4 K) [34]. The high-quality MoS₂/hBN van der Waals heterostructures hence allowed for observing subtle optical and spin-valley properties of monolayer MoS₂ [29, 34, 35].

Recent work reported an observation of a trion line splitting in reflectivity spectra of gated hBN/MoS₂/hBN heterostructures [29], similar to other ‘dark’ TMDs: WSe₂ [36] and WS₂ [37]. Furthermore, numerical calculations of the trion fine structure in doped monolayer MoS₂ by *ab initio* many-body theory show the splitting of the negative trion into three excitations: inter-valley singlet, inter-valley triplet and intra-valley singlet, with a splitting energy of about 1 meV and 4 meV, respectively [27]. Similarly, inter- and intra-valley singlets with 4 meV splitting were predicted [38], along with an unbound intra-valley triplet trion state.

Interestingly, substantially different effective exciton g -factors were determined in hBN-encapsulated MoS₂ monolayers; $g_X = -1.7$ in magneto-photoluminescence experiments [34] and nearly two times higher $g_X = -3.0$ in magneto-transmission measurements [35]. Furthermore, detailed magneto-transmission experiments revealed that the reduced mass of the exciton in monolayer MoS₂ is heavier than predicted by density functional theories [32, 39], suggesting a large electron mass consistent with recent values determined from transport studies of n-type MoS₂ monolayers [40]. The complicated interplay of band structure [32, 41], electron–electron interactions [15, 28, 42, 43], enhanced spin-splitting [44], dynamical effects [45] and inter-/intra-valley phonon [46] and plasmon [24] contributions makes MoS₂ one of the most challenging materials to understand.

In this work we elaborate on the optical properties of van der Waals heterostructures based on the uncapped single-layer MoS₂ stacked onto hBN layers of different thicknesses (MoS₂/hBN) and hBN-encapsulated monolayers (hBN/MoS₂/hBN). We probe their optical properties in the comparative photoluminescence (PL), excitation-photoluminescence and reflectance contrast (RC) measurements. In the optical spectra we identify both the neutral and charged excitons, whose observation is dictated mainly by different two-dimensional electron gas (2DEG) concentrations, also related to the quality of the studied structure. Additionally, for MoS₂/hBN and hBN/MoS₂/hBN structures, which reveal clearly distinct doping levels estimated qualitatively based on the shape of the PL and RC and relative energy position of the exciton and trion resonances, we carry out magneto-PL measurements up to 10 T. We find that the effective exciton g -factor significantly depends on the 2DEG concentration and reaches the lowest value of -2.47 in the hBN-encapsulated structures, which reveal a nearly neutral doping regime. In the uncapped MoS₂ structures the excitonic g -factor varies from -1.15 to -1.39 depending on the thickness of the bottom hBN layer and decreases as a function of rising temperature.

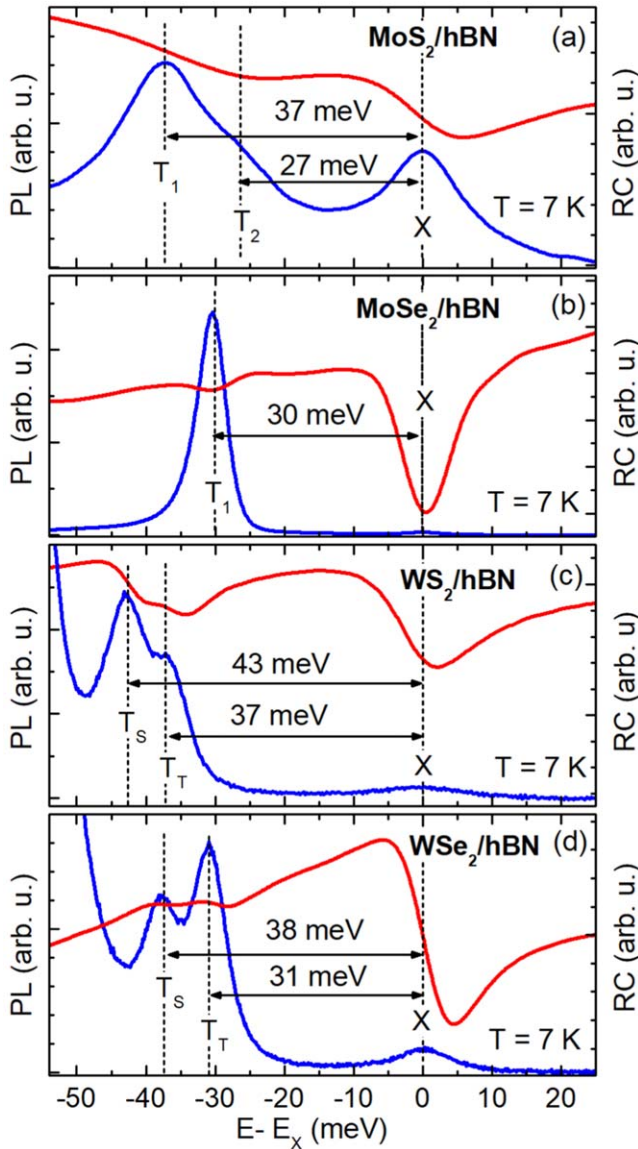


Figure 1. The comparative PL and RC spectra for (a) MoS₂/hBN, (b) MoSe₂/hBN, (c) WS₂/hBN, (d) WSe₂/hBN structures measured at 7 K.

2. Results

2.1. PL and RC measurements of MoS₂, MoSe₂, WS₂ and WSe₂ monolayers

First we discuss results of PL and RC measurements of Mo- and W-based monolayer TMDs. Figures 1(a)–(d) compare low-temperature (7 K) PL and RC spectra of molybdenum- and tungsten-based TMDs monolayers deposited on hBN/SiO₂/Si substrates. The PL spectra are excited non-resonantly at an energy of 2.33 eV. For all monolayers, the optical transitions are associated with the nearly free states of the neutral exciton (X) [20] and different types of trions (T₁, T₂, T_S, T_T) [37, 47], while individual optical transitions positioned at lower energies are not presented. The energy scale of each spectrum is offset with respect to the neutral exciton X. In figure 1(a) we show PL and RC spectra for

MoS₂, while figure 1(b) shows the same spectra for MoSe₂. Interestingly, in the PL spectrum of MoS₂ we see an exciton peak X and two, T₁ and T₂, peaks at lower energies. As indicated in figure 1(a), the energy separation between these optical trion transitions is $\Delta \approx 10$ meV. We attribute them tentatively to the recombination from trion states. The MoS₂ spectra are contrasted with the spectra of MoSe₂, see figure 1(b), which demonstrate an exciton and only a single trion T₁ line. However, the doublet structure of the trion emission line positioned below the neutral exciton in MoS₂ is similar to the trion emission spectra in tungsten-based monolayers, shown in figures 1(c)–(d). In the PL and RC spectra of WS₂ (Figure 1(c)) and WSe₂ (figure 1(d)), the T_S and T_T optical transitions are identified at low doping level ($E_F < E_B$). The energy difference between T_S and T_T is equal to ~ 6 meV, and is in good agreement with the recently reported values [37]. As seen in figures 1(c) and (d), the T_T emission line in the PL spectra of WSe₂ is more prominent than the corresponding optical transition observed in the PL spectra of WS₂. This feature likely depends on the different 2DEG concentrations in the studied monolayers, which in sulfides are typically two orders of magnitude higher than in selenides [33, 48].

2.2. Polarization-resolved PL excitation of trions in monolayer MoS₂

To characterize the nature of the T₁ and T₂ transitions observed in the PL spectra of the MoS₂/hBN structure, we perform polarization-resolved and excitation energy-dependent PL measurements at $T = 7$ K. Figure 2 shows examples of polarization-resolved PL spectra excited strictly resonantly at the neutral exciton energy of 1.9514 eV (figure 2(a)) and near-resonantly at the energy of 1.9730 eV (figure 2(b)). Based on the fitting of the trion contributions to the PL spectrum excited at the neutral exciton energy X (figure 2(a)) with a combination of two Lorentzian curves, we determine the degree of helicity preservation of the emitted light with respect to exciting light defined as $P = (I_{\sigma^+\sigma^+} - I_{\sigma^+\sigma^-}) / (I_{\sigma^+\sigma^+} + I_{\sigma^+\sigma^-})$ for each trion component, where $\sigma^+\sigma^+$ and $\sigma^+\sigma^-$ indicate the co-circular and cross-circular configurations, respectively. The T₁ line displays the P_{T_1} value of almost 66%, while the T₂ line has a slightly higher P_{T_2} of about 72%. For the excitation energy equal to 1.9730 eV (slightly higher than the X energy) we obtain P values of 44%, 46% and 49% for T₁, T₂ and X, respectively (figure 2(b)). We discuss a possible interpretation of those results below.

Additionally, in figures 2(a)–(b) we observe Raman features, which shift as a function of the excitation energy. They are attributed to first- and second-order scattering processes, such as A_1' , E' modes and b , $2LA$ (M) or LA (M) bands, respectively [49, 50]. The presence of the $LA(M)$ band in the Raman scattering spectrum of the MoS₂/hBN heterostructure indicates a considerable amount of defects or disorder in the monolayer [51].

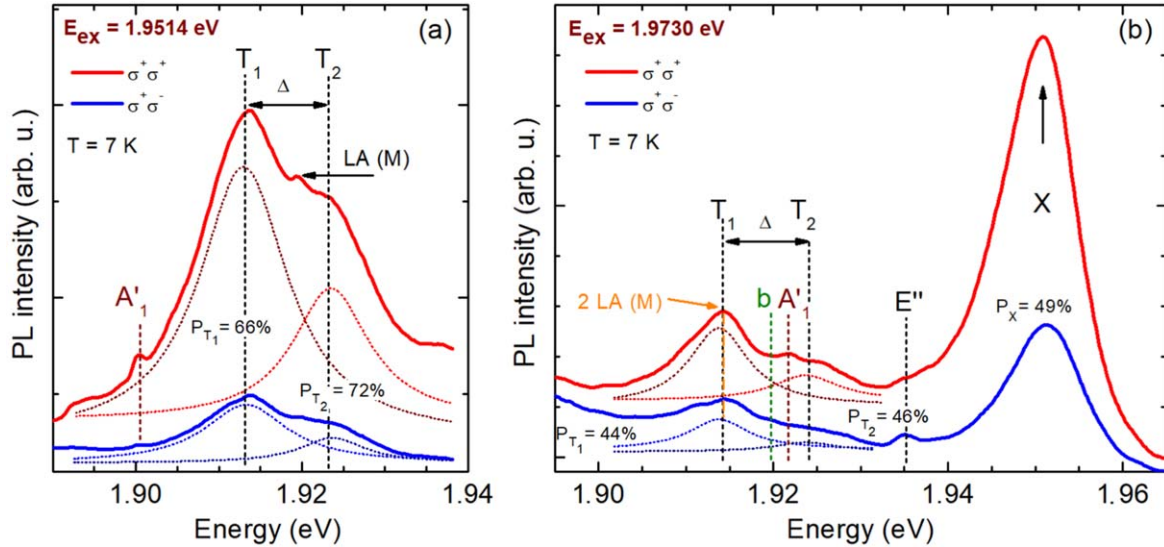


Figure 2. (a) The polarization-resolved PL spectra of MoS₂ excited strictly resonantly at the neutral exciton energy of 1.9514 eV. (b) The resonant circularly polarized PL spectra for 1.9730 eV excitation. The E'', A', b and 2LA (M) indicate the energy position of the Raman features.

2.3. PL and RC spectra in MoS₂/hBN and hBN/MoS₂/hBN heterostructures

In monolayer MoS₂, due to a peculiar arrangement of the conduction bands at the $\pm K$ points, the observation and identification of the fine trion structure in emission spectra are challenging in terms of sample preparation. In this section we discuss the optical properties of MoS₂/hBN and hBN/MoS₂/hBN heterostructures and we show that the relative PL intensity of the T₁ and T₂ features significantly depends on the quality of the sample and doping level.

Figure 3(a) compares low-temperature (7 K) PL (orange, blue and magenta lines) and RC (black line) spectra in the energy range corresponding to the ground state of the neutral and charged excitons for different MoS₂ monolayers: (i) one hBN-encapsulated (hBN/MoS₂/hBN)-f₁ with the thicknesses of the bottom and top hBN layer of ~ 120 nm and ~ 10 nm, respectively, and (ii) two monolayers with only bottom hBN substrate (MoS₂/hBN) with different hBN thickness: f₂-120 nm, f₃-250 nm, correspondingly.

Similarly to our previous studies on WS₂/hBN/SiO₂ heterostructures [26], an extra hBN layer used between the flake and SiO₂/Si substrate acts as a buffer layer and changes the doping level in the monolayer system. It can be explained by the fact that the MoS₂ is naturally n-doped, whereas positively charged defects embedded in SiO₂ strongly influence the electron charge in monolayer MoS₂. Hence, the electron-binding energy to the charged defect embedded in SiO₂ is the largest for MoS₂/SiO₂/Si structures and should decrease with increasing thickness of the hBN layer. Our intuitive explanation is consistent with a recent calculation of ground-state energies of electrons and negative trions in a monolayer supported on SiO₂ as a function of the distance of a positive point-charge defect from the mid-plane of the monolayer [52]. However, there are also different factors which have to be taken into account when the doping is

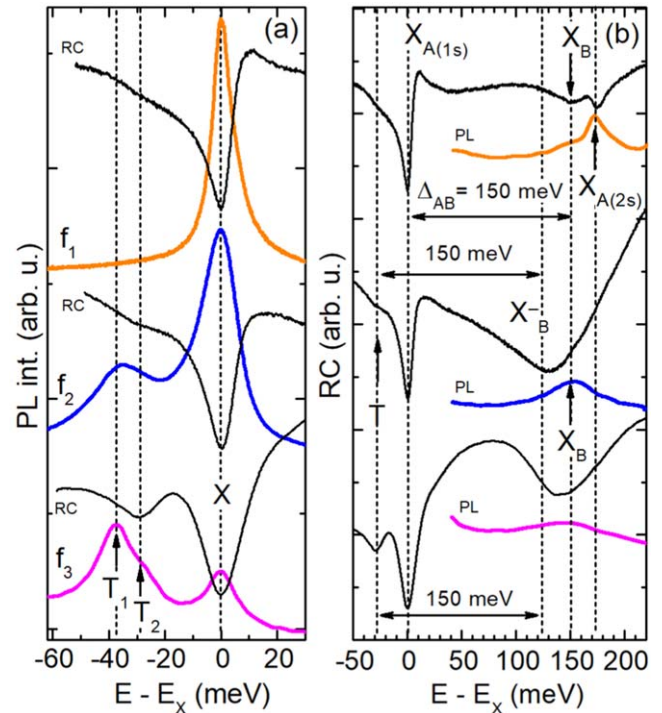


Figure 3. The comparison of low-temperature (7 K) PL and RC spectra for different MoS₂ monolayers: hBN-encapsulated—f₁, and two MoS₂/hBN structures with different thicknesses of hBN layers: f₂-120 nm, f₃-250 nm, respectively. (a) The PL and RC spectra recorded in the vicinity of the excitons (X_{A(1s)}) and trions (T). (b) The PL and RC spectra in the energy range comprising optical transitions assigned to the ground exciton states X_{A(1s)} and X_B, and excited states of the exciton X_{A(1s)}.

estimated. For instance, created defects in the monolayer system can act as donors or acceptors [53, 54] and lead to significant p or n doping. It is also worthwhile to note that the uncapped monolayers are subjected to the photo-doping effects caused by the laser excitation, in contrast to the well

isolated hBN-encapsulated samples. Accordingly, the presented PL spectra reveal relatively different 2DEG concentrations, which are qualitatively estimated by the trion to exciton emission intensity ratio (T/X) [20, 26] and the full-width at half-maximum (FWHM) of neutral exciton. At very low 2DEG concentration, foreseen for the hBN-encapsulated sample (f_1), the X (the FWHM equal to 4meV) line solely dominates the PL spectrum (figure 3(a), orange line), whereas both T lines are not detectable. The same character is also reflected in the complementary RC spectra, dominated by the neutral exciton resonance. At a relatively higher 2DEG concentration (sample f_2 , blue line) a broad T line shows up in the PL spectra, which is likewise accompanied by an emerging trion feature in the RC spectra. For the highest electron doping, as the trion emission intensity exceeds that of a neutral exciton in the f_3 structure (magenta line), the double trion structure becomes quite well resolved in the PL spectrum. Simultaneously, the T resonance in the RC spectrum is more prominent than in the f_1 and f_2 samples and it corresponds to the broader T_2 transition in the PL spectrum. Moreover, in both samples with trion features the FWHM of the X is about two times larger than in the hBN-encapsulated structure. Our observations are consistent with recent results concerning an optical susceptibility measurement of a gated MoS₂ device [29], which also shows that the observation of a well-resolved trion fine structure in optical spectra is a subtle effect, possible only for a particular range of 2DEG concentrations (and also for good sample quality and Ohmic contact), since the linewidth of the higher in energy trion component T_2 significantly increases with increasing electron concentration.

As seen in figure 1(a) the two trions T_1 and T_2 in sample f_3 are redshifted with respect to the neutral exciton X by 37 meV and 27 meV, respectively. From the energy difference between the neutral exciton X and trion T_1 we can evaluate the Fermi level using a formula $\Delta E = E(X) - E(T_1) = E_B + E_F$, where E_B corresponds to the trion binding energy. The T_1 trion binding energy determined in a gated hBN-encapsulated MoS₂ monolayer is equal to 25 meV [29]. In our uncapped MoS₂/hBN heterostructure, due to a change of the dielectric environment the higher trion binding energy is expected. In fact, in the monolayer MoS₂ exfoliated on SiO₂/Si this energy increases up to 30 meV. Hence, we assume that for the well-resolved trion T_1 the binding energy E_B can be in the range from 25 meV to 30 meV. Accordingly, the Fermi level determined from the PL spectrum of the f_3 structure can range from 7 meV to 12 meV. Both the values exceed the theoretically predicted conduction-band spin-splitting in monolayer MoS₂. Then, using equation $n = m_e E_F / \pi \hbar^2$ and the electron effective mass $m_e = 0.44 m_0$ [32, 39], we estimate the intrinsic 2D electron concentration in the range of $1.29\text{--}2.04 \cdot 10^{12} \text{ cm}^{-2}$.

To strengthen our interpretation associated with the different 2DEG concentrations in the presented MoS₂ van der Waals structures, in figure 3(b) we compare PL and RC spectra of all the monolayers at higher energies up to 220 meV above the neutral exciton position. As clearly seen, only in the optical spectra of the hBN-encapsulated sample

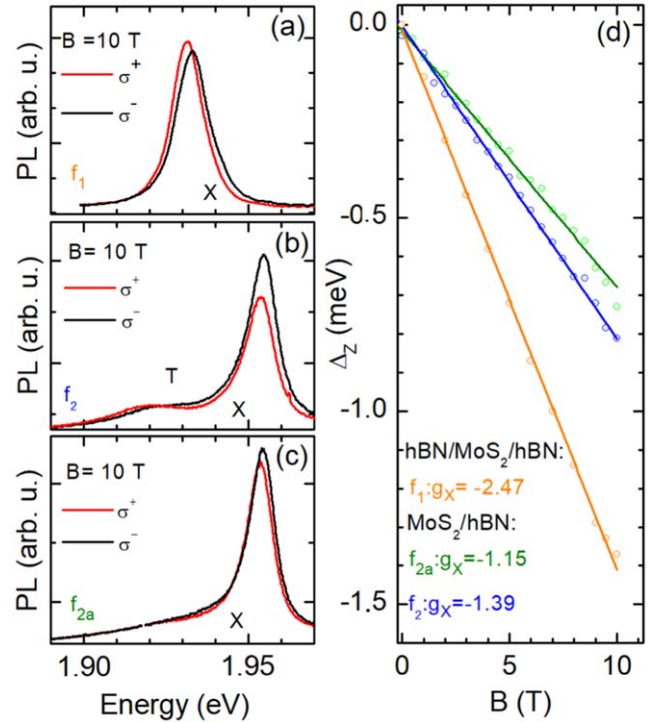


Figure 4. The circularly polarized PL spectra at $B = 10$ T for different MoS₂ monolayers: (a) hBN-encapsulated— f_1 , (b) MoS₂/hBN— f_2 and (c) MoS₂/hBN— f_{2a} . (d) Exciton Zeeman splitting.

(f_1) we can resolve transitions associated with the ground state of the neutral exciton X_B and first excited state of the neutral exciton X_{2s} , which indeed is possible only in the neutral regime doping [55]. The ~ 150 meV energy separation between the X_A and X_B exciton is in line with previous measurements [35, 55] and reflects mostly the spin-orbit splitting of the valence band at the K points of the hexagonal Brillouin zone [6]. For the uncapped MoS₂/hBN heterostructure— f_2 with the same thickness of the bottom hBN layer as in sample f_1 , we observe that the oscillator strength of the neutral X_B exciton is transferred to the negatively charged exciton X_B^- , which confirms a higher electron concentration [55] (note that the energy distance between X_A and X_B and the one between T and X_B^- is the same). Moreover, the high-energy PL spectra of the f_2 and f_3 heterostructures are dominated by the broad X_B emission. The above analysis of the PL and RC shows that the energy separation between the X_A and X_B exciton is similar for all the monolayers and independent of the dielectric environment.

2.4. Zeeman g-factor in monolayer MoS₂

Having estimated the doping levels in the individual MoS₂ monolayers, being (i) very low (or nearly neutral) in the hBN-encapsulated structure, and (ii) relatively higher in the uncapped monolayers, we discuss the magneto-optical response observed in the PL spectra. Figures 4(a)–(c) show the low-temperature (5 K), polarization-resolved PL spectra at $B = 10$ T recorded for one hBN-encapsulated (hBN/MoS₂/hBN)— f_1 and two MoS₂/hBN heterostructures with different hBN thicknesses: f_{2a} —100 nm, f_2 —120 nm,

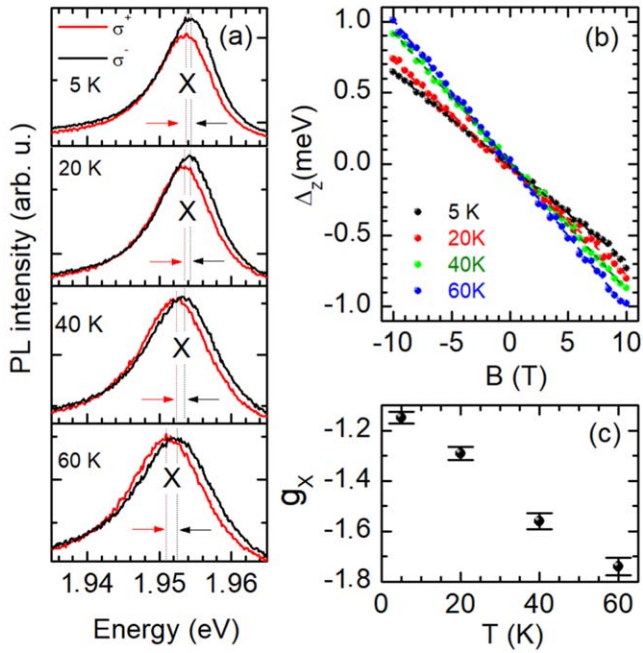


Figure 5. (a) Typical PL spectra of the MoS₂/hBN structure (*f*₂) recorded at 5 K, 20 K, 40 and 60 K. (b) Temperature dependence of exciton Zeeman splitting. (c) Temperature evolution of the effective exciton *g*-factor.

correspondingly. The *f*₂ structure has a slightly higher electron concentration than *f*_{2*a*}, which is reflected by a broad T shoulder. Using non-resonant (2.331 eV) and linearly polarized laser excitation we find that, for the applied magnetic fields, the trion features in samples *f*₂ and *f*_{2*a*} are not sufficiently resolved in the PL spectra to estimate their effective *g*-factors. Accordingly, we focus only on the 2DEG dependence of the exciton *g*-factors.

For figure 4(d), we extracted the Zeeman splitting Δ_Z of the neutral exciton X for all the samples; it is defined as the shift between the σ^+ and σ^- polarized components of the PL: $\Delta_Z = E_{\sigma^+} - E_{\sigma^-} = g_X \mu_B B$. This quantity depends linearly on the magnetic field and our measurements suggest exciton *g*-factors of $g_X = -1.15 \pm 0.01$, $g_X = -1.39 \pm 0.01$, and $g_X = -2.45 \pm 0.01$ for samples *f*_{2*a*}, *f*₂ and *f*₁, respectively. Interestingly, for the MoS₂/hBN structures without a cap layer, the exciton *g*-factor decreases with rising thickness of the hBN layer (with rising 2DEG): *f*_{2*a*}–100 nm, *f*₂–120 nm, respectively. However, for the hBN-encapsulated monolayer MoS₂ (*f*₁) reflecting a nearly neutral doping regime, the exciton *g*-factor is distinct and the lowest.

Furthermore, we probed the temperature dependence of the exciton effective *g*-factor in the MoS₂/hBN structure (*f*_{2*a*}), whose emission spectra are dominated by a relatively narrow X line. Figure 5(a) compares typical PL spectra of the *f*_{2*a*} structure, measured at different temperatures (5 K, 20 K, 40 K, 60 K) and a magnetic field of *B* = 10 T. The exciton Zeeman splitting at four different temperatures is shown in figure 5(b). As seen in figure 5(c), the effective exciton *g*-factor decreases from -1.15 to -1.74 for increasing temperature from 5 K to 60 K. This decrease of the exciton *g*-factor by about 34% is related to the temperature

broadening of the X emission line (see figure 5(a)). However, it may also result from different thermal distributions of electrons in the spin-split subbands. In the hBN-encapsulated monolayer MoS₂ (*f*₁) the temperature effect on the exciton *g*-factor is not observed.

Interestingly, the value of the exciton *g*-factor obtained in our hBN-encapsulated structure ($g_X = -2.45$) lies between values of the *g*-factors determined in recent studies of similar hBN-encapsulated MoS₂ monolayers with very narrow exciton linewidths (2–4 meV), suggesting the exciton *g*-factor of $g_X = -1.7$ [34] in magneto-PL or $g_X = -2.9$ [35] in magneto-transmission experiments. It is worthwhile to mention that the Zeeman splitting, and hence *g*-factors, seem to depend on the doping level and overall optical quality of the sample, which in turn can be mirrored in the linewidth of the PL or RC transitions. However, in comparison to other monolayer TMDs [35, 56], the small exciton Zeeman splitting in the monolayer MoS₂ may arise from the interaction with close in energy, spin- and valley-forbidden, dark excitons. It is noteworthy that semi-dark and dark excitons have been recently identified at 14 meV below the bright states in the PL spectra of hBN-encapsulated MoS₂ placed in transverse and tilted magnetic fields [57]. This bright–dark exciton splitting depends on the spin–orbit splitting of the conduction band, the exciton binding energies and electron–hole exchange interaction. Assuming that an effective exciton *g*-factor reflects the bright–dark exciton interaction, and it can be tuned by the 2DEG concentration and dielectric environment, we tentatively suppose that for different MoS₂/hBN heterostructures the magnitude of this bright–dark splitting can be changed. However, it needs further theoretical calculations.

3. Discussion

Our interpretation of the two emission lines resolved in the spectra of MoS₂, shown in figure 1(a), as originating from two trion states, *T*₁ and *T*₂, is summarized in figures 6(a)–(b). Figure 6(a) shows schematically an electronic configuration for either the inter-valley singlet trion *T*₁, with one spin-up electron in the +*K* valley, a second electron with spin-down and a missing spin-down valence band electron (valence hole) in the –*K* valley or inter-valley triplet, with spin-down electrons in the conduction band. Inter-valley singlet and inter-valley triplet configurations for electrons are denoted by black and red ellipses, respectively. Both columns show single-particle states in +/– *K* valleys on spin–orbit split conduction band states. What is important to understand is that, even though the spin–orbit splitting of the conduction band is ‘bright’, the actual ground excitonic state is ‘dark’, as we have calculated in a recent work by some of the authors [7]. We now explain this bright–dark ground excitonic state inversion. The first mechanism is related to different masses of spin-up and spin-down electrons in the conduction band. The higher energy spin-up conduction band in the –*K* valley is heavier; hence, the higher electron mass combined with electron–hole attraction results in a more strongly bound dark state, pushing the electron–hole bright configuration up in

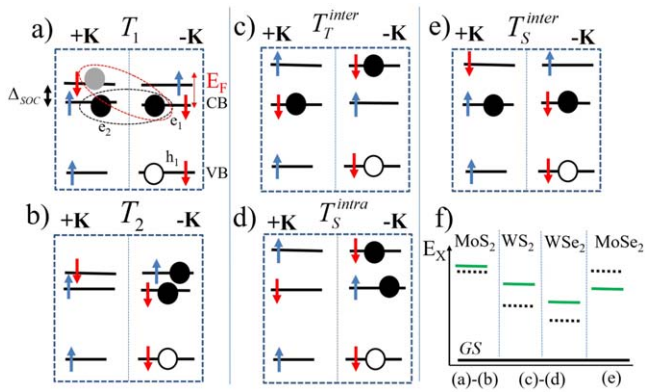


Figure 6. Summary of optically bright trion possibilities in MX_2 on top of single-particle levels in $+K$ and $-K$ valleys (left and right panels, respectively), with only one spin-split valence band shown for clarity. (a) Two possibilities of inter-valley singlet (electron configuration in the conduction band (CB) inside the black dotted ellipsis) and triplet (red ellipsis) and (b) intra-valley singlet trions in material with small CB spin-splitting and dark exciton ground state. (c) Inter-valley triplet and (d) intra-valley singlet trions in material with dark single-particle bands and dark exciton ground state. (e) Inter-valley singlet trion in compounds with bright single-particle bands arrangement and bright exciton ground state. (f) Schematic arrangement of dark (dotted dark lines) and bright (solid green lines) excitonic levels corresponding to (a)–(b), (c)–(d) and (e) single-particle arrangements of carriers.

energy. The second contribution adding to the blue shift of the energy of the bright configuration is the repulsive electron–hole exchange interaction. The two effects result in a splitting of the bright–dark 1s excitons up to 20 meV. Because the starting point is a dark excitonic ground state, we conclude that, for theoretically active trion, two inter-valley configurations are in principle possible, one in singlet and the other with a triplet electron configuration. Those states are predicted to be very close in energy [27], around 1 meV; however, experimental results [29] on a similar structure suggest the inter-valley singlet state interpretation. Additionally, we note that the ordering of the trion states (inter-valley singlet lower than inter-valley triplet) may be reversed due to the interaction of additional carriers in the $+K$ valley with holes in the K valley and small spin–orbit splitting in the conduction band; however, a precise estimation of this effect requires a full many-body calculation of trion states in the presence of a finite carrier concentration in the conduction band, which is still beyond the reach of modern computers due to very strict convergence requirements (as discussed in our recent work [7]). Figure 6(b) shows the configuration of the intra-valley trion where two electrons in the conduction band are in the same $-K$ valley and hence necessarily in the singlet state. An additional possible intra-valley trion state would be an intra-valley triplet trion; however, this state has been shown to be unbound [38]. The assignment of the T_1 line to an inter-valley singlet state and the T_2 line to an intra-valley singlet state is consistent with theoretical calculations [27] and experimental identification of charged complexes [29]. Nevertheless, due to the broad emission feature of the T_1 and T_2 lines, we are not able to exclude the existence of an additional line. The T_1 line may as well be interpreted as an

inter-valley triplet trion, as discussed in [27]; however, gate-tunable device experiments speak against this scenario [29].

The unusual arrangement of the trion states in a material with a positive and small spin–orbit-induced splitting of the conduction band is contrary to trion states in materials with a negative and large spin–orbit-induced splitting of the conduction band such as WS_2 and WSe_2 , see figures 6(c), (d). The single-particle arrangement of levels in the $+K$ valley, left panel in figures 6(c), (d) is opposite to the level arrangement in figures 6(a), (b). There is no inversion of electronic levels for the electron in the presence of valence hole in the $-K$ valley. Hence, the T_T trion is an inter-valley triplet and the lowest energy inter-valley singlet trion is dark, as experimentally confirmed in [58]. The T_S trion is an intra-valley singlet trion. The observation of the doublet structure of bright high-energy trions (T_S , T_T) in WSe_2 and WS_2 monolayers results from the fact that in tungsten-based monolayers the optically active exciton (X) is associated with the top spin-split valence subband (VB) and the upper spin-split conduction subband. Hence, for a low 2DEG concentration, as the electron Fermi level is positioned between the spin-split conduction bands, the triplet trion (figure 6(c)) comprises two electrons from different valleys [59], whereas the singlet trion must involve two electrons from the same valley (figure 6(d)). Additionally, in the simplest case of only one charged complex, the T_S inter-valley trion in MoSe_2 (figure 1(b)) is formed from the optically active exciton associated with the top spin-split valence subband and the lower spin-split conduction subband, see figure 6(e). Accordingly, for the low 2DEG concentration and Fermi level positioned close to the lower spin-split conduction band, the singlet trion should involve two electrons from the different valleys forming the inter-valley spin singlet trion (T_S) with two electrons located in the lower conduction bands. For completeness, in figure 6(f) we summarize the arrangement of bright and dark excitonic levels, underlining that MoS_2 , despite having a ‘bright’ single-particle band arrangement (as for MoSe_2), has a dark excitonic ground state (black dotted lines), as for tungsten-based TMDs.

Now we turn to the discussion of the circular polarization degree results, presented in figure 2. In monolayer TMDs, an exciton circular polarization degree P depends on the specific ratio between the valley depolarization time, controlled mainly by inter-valley electron–hole exchange interaction [60] and the exciton population relaxation time [3]. Precise values of P are however difficult to predict theoretically in realistic devices due to their dependence on defects, substrate and phonon-assisted processes, as well as non-radiative recombination channels [61]. From experimental point of view, it is known that, for MoS_2 , the polarization degree is controlled mainly by the energy of the exciting laser detuned from the exciton resonance [62] and laser power density [63]. Interestingly, both time-resolved and continuous measurements yield similar polarization degrees [63]. For our slightly detuned $E_X = 1.9730$ eV excitation, we obtain 49% polarization degree of the exciton emission, consistent with values reported for time-resolved experiments in [63] and slightly larger than those reported in [34] for a heterostructure similar

to ours. We note that those comments apply to MoS₂, WS₂, WSe₂ TMDs, but for MoSe₂ and MoTe₂ the leading mechanism has been shown to be different [64].

As known from previous studies, a quasi-resonant excitation of the exciton can yield high values of the valley polarization of the trion in MoS₂ [63, 65, 66]. It is generally understood, however, that the effective lifetime of the trion is considerably longer than that of the exciton [3], reaching 70 ps in MoS₂ [67]. Both a high degree of valley polarization as well as a long trion lifetime suggest a very long valley depolarization lifetime, which might be connected to ~100 nanosecond valley coherence of free carriers necessary for the trion formation [68]. However, as for the exciton depolarization problem, theoretical calculations are formidable due to the involvement of a large number of mechanisms [69–71]. Interestingly, the situation gets more complicated when the trion fine structure is involved [72, 73]. For WS₂ and WSe₂ (dark arrangement of bands), different degrees of polarization for intra-valley singlet and inter-valley triplet trions have been reported [73], e.g. 19% and 34% in WS₂, respectively. More recent studies on hBN-encapsulated samples confirmed this difference and showed the dependences of the trion polarization degrees on the laser power [37]. In our experiments (MoS₂ on hBN) which reveal a trion fine structure, we do not observe large differences between the A-exciton resonantly excited (66%, 72%) and quasi-resonantly excited (44% and 46%) polarization degrees of trions, see figure 2. This may suggest that the nature of trion lines is different to that in tungsten-based dark materials. However, the definite conclusion that similar polarization degrees of two lines point towards their identification as inter- and intra-valley singlet trions needs further elaboration.

3.1. Trion splitting as a measure of correlations

Under the assumption of the singlet nature of the T₁ and T₂ trions, we comment on the processes determining their energy splitting. The difference in the total energy of the T₁ and T₂ configurations $E_{T_1} - E_{T_2} = \Delta_{SOC} + V^*$, can be written as a sum of conduction band spin-splitting Δ_{SOC} and electron–electron interactions, V^* . V^* reflects a subtle imbalance between electron–hole and electron–electron interactions inside and between valleys. A simple analysis leads to the expression:

$$V^* = [V^D(e_1, +K; e_2, +K) - V^D(h_1, +K; e_2, +K)] + [V^D(e_1, +K; e_2, -K) - V^D(h_1, +K; e_2, -K)], \quad (1)$$

where $e_{1,2}$ (h_1) describe electrons (holes) forming trions (see figure 6(a)) and V^D is the total direct interaction energy between particles. We see that V^* is the sum of two contributions, a difference between the electron–electron repulsion and electron–hole attraction in the same valley and between valleys. Interestingly, a similar analysis of the singlet-triplet trion splitting in tungsten-based materials leads to $E_{T_S} - E_{T_T} = V^X(e_1, +K; e_2, -K) + V^*$. It suggests that the energy of the singlet–singlet splitting is a new measure for

electronic correlations in 2D crystals with small spin–orbit splitting in conduction bands.

4. Conclusions

In summary, we present results of comparative optical experiments on MoS₂/hBN and hBN/MoS₂/hBN van der Waals heterostructures which reveal a fine structure of the excitonic complexes, whose observation is related to different 2DEG concentrations. In the low-temperature emission spectra of a particular, uncapped MoS₂/hBN heterostructure with the bottom hBN layer thickness of ~250 nm we resolve two trion peaks, T₁ and T₂, resembling the pair of singlet and triplet trion peaks (T_S and T_T) in tungsten-based materials. The existence of these trion features suggests that monolayer MoS₂ has a dark excitonic ground state, despite having a ‘bright’ single-particle arrangement of spin-polarized conduction bands. In addition to that, we show that the effective excitonic g -factor significantly depends on the doping level and reaches the lowest value of -2.47 in the hBN-encapsulated structures indicating a nearly neutral doping regime. In the uncapped MoS₂ structures the excitonic g -factor varies from -1.15 to -1.39 depending on the thickness of the bottom hBN layer and decreases as a function of rising temperature.

Acknowledgments

JJ, JK-G and LB acknowledge support by the Polish NCN Grant ‘Beethoven 2’ No. 2016/23/G/ST3/04114. JD and JJS acknowledge support by the German DFG ‘Beethoven 2’ Grant No. DE 2206/2-1. MB and PH thank P L Lo, S J Cheng, NCTU Taiwan and L Szulakowska, uOttawa for discussions. MB and PH acknowledge support from NSERC Discovery and QC2DM Strategic Project grants as well as uOttawa Research Chair in Quantum Theory of Materials, Nanostructures and Devices. AW and MB acknowledge financial support from the National Science Center (NCN), Poland, grant Maestro No. 2014/14/A/ST3/00654. Computing resources from Compute Canada and Wroclaw Center for Networking and Supercomputing are gratefully acknowledged. TK and P K acknowledge support from the ATOMOPTO project carried out within the TEAM programme of the Foundation for Polish Science co-financed by the European Union under the European Regional Development Fund.

ORCID iDs





J Jadcak  <https://orcid.org/0000-0003-2953-1203>

J Kutrowska-Girzycka  <https://orcid.org/0000-0002-0480-444X>

T Kazimierczuk  <https://orcid.org/0000-0001-6545-4167>

P Kossacki  <https://orcid.org/0000-0002-7558-1044>

J J Schindler  <https://orcid.org/0000-0001-9542-1040>

J Debus  <https://orcid.org/0000-0002-8678-4402>
 K Watanabe  <https://orcid.org/0000-0003-3701-8119>
 C H Ho  <https://orcid.org/0000-0002-7195-208X>
 L Bryja  <https://orcid.org/0000-0001-5211-581X>

References

- [1] Geim A K and Grigorieva I V 2013 Van der Waals heterostructures *Nature* **499** 419
- [2] Mak K F, Xiao D I and Shan J 2018 Light-valley interactions in 2D semiconductors *Nat. Photonics* **12** 451
- [3] Wang G, Chernikov A, Glazov M M, Heinz T F, Marie X, Amand T and Urbaszek B 2018 Colloquium: Excitons in atomically thin transition metal dichalcogenides *Rev. Mod. Phys.* **90** 021001
- [4] Mak K F, Lee C, Hone J, Shan J and Heinz T F 2010 Atomically thin MoS₂: a new direct-gap semiconductor *Phys. Rev. Lett.* **105** 136805
- [5] Xiao D, Liu G-B, Feng W, Xu X and Yao W 2012 Coupled spin and valley physics in monolayers of MoS₂ and other group-VI dichalcogenides *Phys. Rev. Lett.* **108** 196802
- [6] Zhu Z Y, Cheng Y C and Schwingenschlögl U 2011 Giant spin-orbit-induced spin splitting in two-dimensional transition-metal dichalcogenide semiconductors *Phys. Rev. B* **84** 153402
- [7] Bieniek M, Szulakowska L and Hawrylak P 2020 Band nesting and exciton spectrum in monolayer MoS₂ *Phys. Rev. B* **101** 125423
- [8] Qiu D Y, da Jornada F H and Louie S G 2013 Optical spectrum of MoS₂: Many-body effects and diversity of exciton states *Phys. Rev. Lett.* **111** 216805
- [9] Yu H, Laurien M, Hu Z and Rubel O 2019 Exploration of the bright and dark exciton landscape and fine structure of MoS₂ using g₀w₀-bse *Phys. Rev. B* **100** 125413
- [10] Molas M R, Faugeras C, Slobodeniuk A O, Nogajewski K, Bartos M, Basko D M and Potemski M 2017 Brightening of dark excitons in monolayers of semiconducting transition metal dichalcogenides *2D Materials* **4** 021003
- [11] Dingle R, Wiegmann W and Henry C H 1974 Quantum states of confined carriers in very thin Al_xGa_{1-x}As-GaAs-Al_xGa_{1-x}As heterostructures *Phys. Rev. Lett.* **33** 827-30
- [12] Jadcak J, Bryja L, Wójs A and Potemski M 2012 Optically induced charge conversion of coexistent free and bound excitonic complexes in two-beam magnetophotoluminescence of two-dimensional quantum structures *Phys. Rev. B* **85** 195108
- [13] Lampert M A 1958 Mobile and immobile effective-mass-particle complexes in nonmetallic solids *Phys. Rev. Lett.* **1** 450-3
- [14] Kheng K, Cox R T, d'Aubigné M Y, Bassani F, Saminadayar K and Tatarenko S 1993 Observation of negatively charged excitons X⁻ in semiconductor quantum wells *Phys. Rev. Lett.* **71** 1752-5
- [15] Hawrylak P 1991 Optical properties of a two-dimensional electron gas: Evolution of spectra from excitons to Fermi-edge singularities *Phys. Rev. B* **44** 3821-8
- [16] Bryja L, Jadcak J, Wójs A, Bartsch G, Yakovlev D R, Bayer M, Plochocka P, Potemski M, Reuter D and Wieck A D 2012 Cyclotron-resonant exciton transfer between the nearly free and strongly localized radiative states of a two-dimensional hole gas in a high magnetic field *Phys. Rev. B* **85** 165308
- [17] Jadcak J, Kubisa M, Ryczko K, Bryja L and Potemski M 2012 High magnetic field spin splitting of excitons in asymmetric GaAs quantum wells *Phys. Rev. B* **86** 245401
- [18] Narvaez G A, Hawrylak P and Brum J A 2001 The role of finite hole mass in the negatively charged exciton in two dimensions *Physica E* **9** 716-22
- [19] Mak K F, He K, Lee C, Lee G H, Hone J, Heinz T F and Shan J 2013 Tightly bound trions in monolayer MoS₂ *Nat. Mater.* **12** 207-11
- [20] Jadcak J, Kutrowska-Girzycka J, Kapuściński P, Huang Y S, Wójs A and Bryja L 2017 Probing of free and localized excitons and trions in atomically thin WSe₂, WS₂, MoSe₂ and MoS₂ in photoluminescence and reflectivity experiments *Nanotechnology* **28** 395702
- [21] Jadcak J, Delgado A, Bryja L, Huang Y S and Hawrylak P 2017 Robust high-temperature trion emission in monolayers of Mo(S_ySe_{1-y})₂ alloys *Phys. Rev. B* **95** 195427
- [22] Hawrylak P 1990 Optical hole in a two-dimensional electron gas *Phys. Rev. B* **42** 8986-90
- [23] Brown S A, Young J F, Brum J A, Hawrylak P and Wasilewski Z 1996 Evolution of the interband absorption threshold with the density of a two-dimensional electron gas *Phys. Rev. B* **54** R11082-5
- [24] Van Tuan D, Scharf B, Žutić I and Dery H 2017 Marrying excitons and plasmons in monolayer transition-metal dichalcogenides *Phys. Rev. X* **7** 041040
- [25] Van Tuan D, Scharf B, Wang Z, Shan J, Mak K F, Žutić I and Dery H 2019 Probing many-body interactions in monolayer transition-metal dichalcogenides *Phys. Rev. B* **99** 085301
- [26] Jadcak J, Bryja L, Kutrowska-Girzycka J, Kapuscinski P, Bieniek M, Huang Y-S and Hawrylak P 2019 Room temperature multi-phonon upconversion photoluminescence in monolayer semiconductor WS₂ *Nat. Commun.* **10** 107
- [27] Drüppel M, Deilmann T, Krüger P and Rohlfing M 2017 Diversity of trion states and substrate effects in the optical properties of an MoS₂ monolayer *Nat. Commun.* **8** 2117
- [28] Scrace T, Tsai Y, Barman B, Schweidenback L, Petrou A, Kioseoglou G, Ozfidan I, Korkusinski M and Hawrylak P 2015 Magnetoluminescence and valley polarized state of a two-dimensional electron gas in WS₂ monolayers *Nat. Nanotechnol.* **10** 603-7
- [29] Roch J G, Froehlicher G, Leisgang N, Makk P, Watanabe K, Taniguchi T and Warburton R J 2019 Spin-polarized electrons in monolayer MoS₂ *Nat. Nanotechnol.* **14** 432-6
- [30] Connell G A N, Wilson J A and Yoffe A D 1969 Effects of pressure and temperature on exciton absorption and band structure of layer crystals: molybdenum disulphide *J. Phys. Chem. Solids* **30** 287-96
- [31] Anthony J W, Bideaux R A, Bladh K W and Nichols M C 2014 *Handbook of Mineralogy* (Chantilly, VA: Mineralogical Society of America) 20151-1110, USA
- [32] Kadantsev E S and Hawrylak P 2012 Electronic structure of a single MoS₂ monolayer *Solid State Commun.* **152** 909
- [33] Radisavljevic B, Radenovic A, Brivio J, Giacometti V and Kis A 2011 Single-layer MoS₂ transistors *Nat. Nano.* **6** 14750
- [34] Cadiz F *et al* 2017 Excitonic linewidth approaching the homogeneous limit in MoS₂-based van der Waals heterostructures *Phys. Rev. X* **7** 021026
- [35] Goryca M *et al* 2019 Revealing exciton masses and dielectric properties of monolayer semiconductors with high magnetic fields *Nat. Commun.* **10** 4172
- [36] Lyons T P, Dufferwiel S, Brooks M, Withers F, Taniguchi T, Watanabe K, Novoselov K S, Burkard G and Tartakovskii A I 2019 The valley Zeeman effect in inter- and intra-valley trions in monolayer WSe₂ *Nat. Commun.* **10** 2330
- [37] Vaclavkova D, Wyzula J, Nogajewski K, Bartos M, Slobodeniuk A O, Faugeras C, Potemski M and Molas M R 2018 Singlet and triplet trions in WS₂ monolayer encapsulated in hexagonal boron nitride *Nanotechnology* **29** 325705

- [38] Tempelaar R and Berkelbach T C 2019 Many-body simulation of two-dimensional electronic spectroscopy of excitons and trions in monolayer transition metal dichalcogenides *Nat. Commun.* **10** 3419
- [39] Kormányos A, Burkard G, Gmitra M, Fabian J, Zólyomi V, Drummond N D and Fal'ko V 2015 kp theory for two-dimensional transition metal dichalcogenide semiconductors *2D Materials* **2** 022001
- [40] Pisoni R et al 2018 Interactions and magnetotransport through spin-valley coupled Landau levels in monolayer MoS₂ *Phys. Rev. Lett.* **121** 247701
- [41] Bieniek M, Korkusiński M, Szulakowska L, Potasz P, Ozfidan I and Hawrylak P 2018 Band nesting, massive Dirac fermions, and valley Landé and Zeeman effects in transition metal dichalcogenides: A tight-binding model *Phys. Rev. B* **97** 085153
- [42] Efimkin D K and MacDonald A H 2017 Many-body theory of trion absorption features in two-dimensional semiconductors *Phys. Rev. B* **95** 035417
- [43] Gao S and Yang L 2017 Renormalization of the quasiparticle band gap in doped two-dimensional materials from many-body calculations *Phys. Rev. B* **96** 155410
- [44] Ferreiros Y and Cortijo A 2014 Large conduction band and Fermi velocity spin splitting due to Coulomb interactions in single-layer MoS₂ *Phys. Rev. B* **90** 195426
- [45] Liu F, Ziffer M E, Hansen K R, Wang J and Zhu X 2019 Direct determination of band-gap renormalization in the photoexcited monolayer MoS₂ *Phys. Rev. Lett.* **122** 246803
- [46] Glazov M M, Semina M A, Robert C, Urbaszek B, Amand T and Marie X 2019 Intervalley polaron in atomically thin transition metal dichalcogenides *Phys. Rev. B* **100** 041301
- [47] Courtade E et al 2017 Charged excitons in monolayer WSe₂: experiment and theory *Phys. Rev. B* **96** 085302
- [48] Ross J S et al 2013 Electrical control of neutral and charged excitons in a monolayer semiconductor *Nat. Commun.* **4** 1474
- [49] Molas M R, Golasa K, Bala L, Nogajewski K, Bartos M, Potemski M and Babinski A 2019 Tuning carrier concentration in a superacid treated MoS₂ monolayer *Sci. Rep.* **9** 1989
- [50] Kutrowska-Girzycka J, Jadcak J and Bryja L 2018 The study of dispersive 'b'-mode in monolayer MoS₂ in temperature dependent resonant Raman scattering experiments *Solid State Commun.* **275** 25–8
- [51] Mignuzzi S, Pollard A J, Bonini N, Brennan B, Gilmore I S, Pimenta M A, Richards D and Roy D 2015 Effect of disorder on Raman scattering of single-layer MoS₂ *Phys. Rev. B* **91** 195411
- [52] Van Tuan D, Jones A M, Yang M, Xu X and Dery H 2019 Virtual trions in the photoluminescence of monolayer transition-metal dichalcogenides *Phys. Rev. Lett.* **122** 217401
- [53] Lin Y et al 2015 Three-fold rotational defects in two-dimensional transition metal dichalcogenides *Nat. Commun.* **6** 6736
- [54] Santosh K C, Longo R C, Addou R, Wallace R M and Cho K 2014 Impact of intrinsic atomic defects on the electronic structure of MoS₂ monolayers *Nanotechnology* **25** 375703
- [55] Robert C et al 2018 Optical spectroscopy of excited exciton states in MoS₂ monolayers in van der Waals heterostructures *Phys. Rev. Materials* **2** 011001
- [56] Koperski M, Molas M R, Arora A, Nogajewski K, Bartos M, Wyzula J, Vaclavkova D, Kossacki P and Potemski M 2018 Orbital, spin and valley contributions to Zeeman splitting of excitonic resonances in MoSe₂, WSe₂ and WS₂ monolayers *2D Materials* **6** 015001
- [57] Robert C et al 2020 Measurement of the spin-forbidden dark excitons in MoS₂ and MoSe₂ monolayers *Nat. Commun.* **11** 4037
- [58] Volmer F, Pissinger S, Ersfeld M, Kuhlen S, Stampfer C and Beschoten B 2017 Intervalley dark trion states with spin lifetimes of 150 ns in WSe₂ *Phys. Rev. B* **95** 235408
- [59] Yu H, Cui X, Xu X and Yao W 2015 Valley excitons in two-dimensional semiconductors *Nat. Sci. Rev.* **2** 57–70
- [60] Yu T and Wu M W 2014 Valley depolarization due to intervalley and intravalley electron-hole exchange interactions in monolayer MoS₂ *Phys. Rev. B* **89** 205303
- [61] Wang G H W et al 2012 Valley-selective circular dichroism of monolayer molybdenum disulfide *Nat. Commun.* **3** 887
- [62] Hanbicki A C M et al 2016 Optical polarization and intervalley scattering in single layers of MoS₂ and MoSe₂ *Sci Rep* **6** 25041
- [63] Lagarde D, Bouet L, Marie X, Zhu C R, Liu B L, Amand T, Tan P H and Urbaszek B 2014 Carrier and polarization dynamics in monolayer MoS₂ *Phys. Rev. Lett.* **112** 047401
- [64] Yang M, Robert C, Lu Z, Van Tuan D, Smirnov D, Marie X and Dery H 2020 Exciton valley depolarization in monolayer transition-metal dichalcogenides *Phys. Rev. B* **101** 115307
- [65] Mak K F, He K, Shan J and Heinz T F 2012 Control of valley polarization in monolayer MoS₂ by optical helicity *Nat. Nanotechnol.* **7** 494–8
- [66] Zeng H, Dai J, Yao W, Xiao D and Cui X 2012 Valley polarization in MoS₂ monolayers by optical pumping *Nat. Nanotechnol.* **7** 490–3
- [67] Zhang W, Tanaka K, Hasegawa Y, Shinokita K, Matsuda K and Miyauchi Y 2020 Bright and highly valley polarized trions in chemically doped monolayer MoS₂ *Applied Physics Express* **13** 035002
- [68] Yang L, Sinitsyn N A, Chen W, Yuan J, Zhang J, Lou J and Crooker S A 2015 Long-lived nanosecond spin relaxation and spin coherence of electrons in monolayer MoS₂ and WS₂ *Nat. Phys.* **11** 830–4
- [69] Shinokita K, Wang X, Miyauchi Y, Watanabe K, Taniguchi T, Konabe S and Matsuda K 2019 Phonon-mediated intervalley relaxation of positive trions in monolayer WSe₂ *Phys. Rev. B* **100** 161304
- [70] Hao K et al 2017 Trion valley coherence in monolayer semiconductors *2D Materials* **4** 025105
- [71] Singh A et al 2016 Long-lived valley polarization of intravalley trions in monolayer WSe₂ *Phys. Rev. Lett.* **117** 257402
- [72] Jones A M, Yu H, Schaibley J R, Yan J, Mandrus D G, Taniguchi T, Watanabe K, Dery H, Yao W and Xu X 2016 Excitonic luminescence upconversion in a two-dimensional semiconductor *Nat. Phys.* **12** 323–7
- [73] Plechinger G, Nagler P, Arora A, Schmidt R, Chernikov A, del Águila A G, Christianen P C M, Bratschkitsch R, Schüller C and Korn T 2016 Trion fine structure and coupled spin-valley dynamics in monolayer tungsten disulfide *Nat. Commun.* **7** 12715